International Journal of Pharmaceutics 630 (2023) 122462

Contents lists available at ScienceDirect

International Journal of Pharmaceutics

journal homepage: www.elsevier.com/locate/ijpharm

In vivo assessment of tumor targeting potential of ^{68}Ga-labelled randomly methylated beta-cyclodextrin (RAMEB) and 2-hydroxypropyl-β-cyclodextrin (HPβCD) using positron emission tomography

Judit P. Szabó [a,b], Katalin Csige [a,c], Ibolya Kálmán-Szabó [a,d], Viktória Arató [a,d], Gábor Opposits [a], István Jószai [a], István Kertész [a], Zita Képes [a], Gábor Méhes [e], Ferenc Fenyvesi [f], István Hajdu [a,1], György Trencsényi [a,b,d,1,*]

[a] Division of Nuclear Medicine and Translational Imaging, Department of Medical Imaging, Faculty of Medicine, University of Debrecen, Nagyerdei St. 98, H-4032 Debrecen, Hungary
[b] Doctoral School of Clinical Medicine, Faculty of Medicine, University of Debrecen, Nagyerdei St. 98, H-4032, Debrecen, Hungary
[c] Doctoral School of Pharmaceutical Sciences, University of Debrecen, Nagyerdei St. 98, H-4032 Debrecen, Hungary
[d] Gyula Petrányi Doctoral School of Allergy and Clinical Immunology, Faculty of Medicine, University of Debrecen, Nagyerdei St. 98, H-4032, Debrecen, Hungary
[e] Department of Pathology, Faculty of Medicine, University of Debrecen, Nagyerdei St. 98, H-4032 Debrecen, Hungary
[f] Department of Pharmaceutical Technology, Faculty of Pharmacy, University of Debrecen, Nagyerdei St. 98, H-4032 Debrecen, Hungary

ARTICLE INFO

Keywords:
^{68}Ga
Cyclodextrin
Positron Emission Tomography
prostaglandin E2

ABSTRACT

Cyclodextrin derivates (CyDs) can form complexes with cyclooxygenase-2 induced tumor promoting prostaglandin E2 (PGE2). Based on our previous observations, ^{68}Ga-labelled CyDs may represent promising radiopharmaceuticals in the positron emission tomography (PET) diagnostics of PGE2 positive tumors. We aimed at evaluating the tumor-targeting potential of ^{68}Ga-NODAGA conjugated randomly methylated beta-cyclodextrin (^{68}Ga-NODAGA-RAMEB) and 2-hydroxypropyl-β-cyclodextrin (^{68}Ga-NODAGA-HPβCD) using *in vivo* PET imaging with experimental tumor models. Tumor radiopharmaceutical uptake was assessed applying PET and gamma counter *in vivo* and *ex vivo* respectively, following the administration of ^{18}FDG, ^{68}Ga-NODAGA-RAMEB or ^{68}Ga-NODAGA-HPβCD *via* the lateral tail vein to the subsequent tumor-bearing animals: HT1080, A20, PancTu-1, BxPC3, B16-F10, Ne/De and He/De. All investigated tumors were identifiable with both ^{68}Ga-labelled CyDs; however, *in vivo* results, in correlation with the *ex vivo* data, revealed that the PGE2 positive BxPC3, A20, Ne/De and He/De tumors presented the highest accumulation. In case of HT1080, A20, B16-F10 tumors significant differences were encountered between the accumulations of both ^{68}Ga-labelled radiopharmaceuticals of the same tumor. Subcutaneously and the orthotopically transplanted Ne/De tumors differed significantly ($p \leq 0.01$) regarding tracer uptake. ^{68}Ga-labelled CyDs may open a novel field in the PET diagnostics of PGE2 positive primary tumors and metastases.

Abbreviations: CyDs, cyclodextrins; DAB, diaminobenzidine; EP, E-type prostanoid receptor; ^{18}FDG, [^{18}F]2-fluoro-2-deoxy-D-glucose; H&E, hematoxylin-eosin; HPβCD, (2-Hydroxypropyl)-β-cyclodextrin; NODAGA, p-NCS-benzyl-NODA-GA; PET, positron emission tomography; PGE2, prostaglandin E2; PTLN, parathymic lymph node; RAMEB, randomly methylated β-cyclodextrin; SRCA, subrenal capsule assay; SUV, standardised uptake value; T/M, tumor-to-muscle ratio; VOI, volume of interest.

* Corresponding author at: Division of Nuclear Medicine and Translational Imaging, Department of Medical Imaging, Faculty of Medicine, University of Debrecen, Nagyerdei St. 98, H-4032 Debrecen, Hungary.
E-mail address: trencsenyi.gyorgy@med.unideb.hu (G. Trencsényi).
[1] These authors contributed equally to this study.

https://doi.org/10.1016/j.ijpharm.2022.122462
Received 29 June 2022; Received in revised form 21 November 2022; Accepted 27 November 2022
Available online 30 November 2022

1. Introduction

Nowadays, several data illustrating the ever-increasing prevalence of malignant diseases have re-ignited the interest in widening the *in vivo* diagnostic armamentarium of different cancers. With the development of molecular biology, more and more potential tumor markers are being discovered and the number of new tumor-specific diagnostic molecules is increasing accordingly.

Cyclodextrins (CyDs) have recently come to the forefront of nuclear medicine as potential tumor-targeting molecules. These glucose-based cyclic oligosaccharides possessing a hydrophilic external surface and a lipophilic inner cavity have been pinpointed to be promising tools to prepare endocytosis-based drug delivery systems and develop water soluble drugs (Duchene et al., 2016, Loftsson et al., 2005, Szejtli, 1998). A long list of chemically modified CyDs with improved inclusion capability and physicochemical characteristics has been synthesized to make them able to create compounds with different types of molecules (Sauer et al., 2017). Given the aforementioned favourable chemical properties, CyDs and their radiolabelled derivates might open a novel field in the *in vivo* molecular imaging of malignancies.

Positron emission tomography (PET) is considered to be the mainstream *in vivo* healthcare tool in the identification of primary malignancies, and their metastases as well as the evaluation of novel anticancer therapeutic products. To understand the not yet fully elucidated neoplastic *in vivo* pathways, several types of PET radiotracers have been introduced. For the labelling of different tumor-related molecules - including CyDs - positron emitter Gallium-68 (^{68}Ga) characterised by a half-life of 68 min is a frequently utilised radiometal (Hajdu et al., 2019). In our previous study it was reported that ^{68}Ga is a suitable radionuclide for the labelling of CyD derivates, furthermore, the specific binding of ^{68}Ga-labelled CyDs to prostaglandin E2 (PGE2) overexpressing tumors was also demonstrated (Trencsényi et al., 2020).

Among CyD derivates the randomly methylated β-cyclodextrin (RAMEB) was reported to express high affinity to form complexes with PGE2 that has a crucial role in cancer formation *via* the cyclooxygenase-2 (COX-2)/prostaglandin E2 (PGE2) pathway (Karpisheh et al., 2019, Sauer et al., 2017). Within the framework of a preclinical experiment using PGE2 positive tumor bearing mice, RAMEB CyD was labelled with 1,4,7-triazacyclononane,1-glutaric acid-4,7-acetic acid (NODAGA) bifunctional chelator and positron emitting ^{68}Ga radiometal, making the resulting ^{68}Ga-NODAGA-RAMEB probe bound to the tumor with high efficacy purveying the basis for PGE2-targeted *in vivo* PET imaging (Trencsényi et al., 2020).

Besides RAMEB, hydroxypropyl-beta-cyclodextrin (HPβCD) has already gained notable clinical attention in therapeutic routes due to its efficacy, satisfactory safety profile and measurable tolerability (Gould and Scott, 2005, Hastings et al., 2019). Intravenously administered HPβCD-diclofenac complex has proved to be an efficacious post-operative pain killer (Chelly et al., 2013). Moreover, HPβCD revolutionised the treatment of the rare, neurodegenerative genetic disorder, Niemann-Pick disease type C1 (NPC1) (Ottinger et al., 2014). Preclinical studies with the enrollment of NPC1 mouse and cat receiving HPβCD, revealed considerable delay in the progression of NPC1-associated neurological symptoms and demonstrated prolongation of lifespan (Davidson et al., 2009, Vite et al., 2015). ^{68}Ga-labelled NODAGA-HPβCD (^{68}Ga-NODAGA-HPβCD) was synthesized for the first time by Hajdu *et al.* in 2019 (Hajdu et al., 2019). The newly synthesized ^{68}Ga-NODAGA-HPβCD represents a new area of investigations in the field of biomedical and pharmaceutical research. Another significant aspect is that the pre-eminent *in vivo* biodistribution and pharmacokinetics of ^{68}Ga-NODAGA-HPβCD, as well as its high radiochemical purity may ensure opportunities for further pharmacokinetic measurements, and may also be relevant for tumor-specific molecular imaging (Hajdu et al., 2019).

The above detailed previously published data inspired us to investigate the diagnostic value of CyD derivates in the molecular imaging of different neoplasms that may bring us closer to the ultimate goal of molecular target-based cancer therapy. Therefore, herein we aimed to assess the tumor-targeting potential of ^{68}Ga-NODAGA-RAMEB and ^{68}Ga-NODAGA-HPβCD using non-invasive *in vivo* PET imaging.

2. Materials and methods

2.1. Chemicals

6-monodeoxy-6-monoamino-randomly-methylated-beta-cyclodextrin hydrochloride (NH_2-RAMEB) and 6-deoxy-6-monoamino-(2-Hydroxypropyl)-β-cyclodextrin (NH_2-HPβCD) were produced by CycloLab ltd. (Budapest, Hungary). p-NCS-benzyl-NODA-GA (NODAGA) was obtained from CheMatech (Cat. No.:C103) (Dijon, France). Both for the chemical synthesis and the radiolabelling procedures, dimethyl sulfoxide (DMSO), *N,N*-Diisopropylethylamine (DIPEA), ACS grade water and ammonium acetate (NH_4OAc) were purchased from Sigma-Aldrich ltd. (Budapest, Hungary). Ultra-pure (u.p.) HCl was the product of Merck ltd. (Budapest, Hungary). All other chemicals were purchased from VWR International ltd. (Debrecen, Hungary) and Sigma-Aldrich ltd. (Budapest, Hungary). [^{18}F]2-fluoro-2-deoxy-D-glucose (^{18}FDG) is routinely produced in the Department of Nuclear Medicine (University of Debrecen, Debrecen, Hungary) for human PET imaging in accordance with GMP regulations.

2.2. ^{68}Ga-labelling of NODAGA-RAMEB and NODAGA-HPβCD

The ^{68}Ga-labelling methodology of the NODAGA-HPβCD and NODAGA-RAMEB CyDs was described earlier (Hajdu et al., 2019; Trencsényi et al., 2020). Briefly, for the 68 Ga production a 68Ge/68 Ga generator (Hajdu et al., 2019; Trencsényi et al., 2020). Briefly, for the ^{68}Ga production a ^{68}Ge/^{68}Ga generator (50 mCi, Gallia-Pharm, Eckert and Ziegler Germany) was used. The eluted ^{68}Ga aliquot (1 mL) was buffered with 1 M sodium acetate, followed by the addition of an aqueous solution of 1 mM of NODAGA-RAMEB or NODAGA- HPβCD. After heating the reaction mixture (10 min at 95 °C), the solution was transferred to a Light C18 Sep-Pak Cartridge and washed with water (2 mL) to remove the buffer. The ^{68}Ga-labelled products were eluted with 96 % EtOH/isotonic NaCl solution and the radiochemical purity was evaluated by a HPLC system with Supelco Discovery® Bio Wide Pore C-18 column (250 mm × 4.6 mm; particle size: 10 μm) combined with a radiodetector. Signals were simultaneously detected by radio and absorbance detector at 254 nm. Before the animal experiments, the product was diluted with saline to reduce the ethanol content below 10 %, and then filtered to be sterile.

2.3. Determination of in vitro and in vivo metabolic stability

The *in vitro* stability of ^{68}Ga-NODAGA-HPβCD and ^{68}Ga-NODAGA-RAMEB was investigated in mouse serum separately. ^{68}Ga-NODAGA-HPβCD (10 μL, 6 ± 0.4 MBq) and ^{68}Ga-NODAGA-RAMEB (10 μL, 5 ± 0.6 MBq) were incubated in mouse serum at 37 °C without stirring. 50 μL aliquots from this mixture were mixed with 50 μL ice cold abs. ethanol at different time points (30, 60 and 90 min). The mixture was then centrifuged at 4°C than the supernatant was collected and evaluated by analytical radio-HPLC. For the determination of *in vivo* metabolic stability 12-week-old healthy SCID mice were used. Samples of ^{68}Ga-NODAGA-HPβCD (10 ± 0.3 MBq) and ^{68}Ga-NODAGA-RAMEB (10 ± 0.4 MBq) were injected into mice via the lateral tail vein. After 60 min incubation time 50 μL urine samples were mixed with ice-cold abs ethanol and centrifuged at 4 °C for 5 min. The supernatant was also evaluated by analytical radio-HPLC. In all cases, the HPLC chromatograms were compared with the initial chromatograms of the radiotracer to detect the presence of any radioactive metabolites.

2.4. Cell culturing

HT1080 (human fibrosarcoma), A20 (mouse B cell lymphoma), PancTu-1 and BxPC3 (human pancreas adenocarcinoma), and B16-F10 (mouse melanoma) cells lines were purchased from ATCC (Virginia, USA). Ne/De (rat mesoblastic nephroma) and He/De (rat hepatocellular carcinoma) cell lines were established at the University of Debrecen (14). The used cell lines were cultured in GlutaMAX ™ DMEM (Gibco™) supplemented with antimicotic-antibiotic solution (1 % (vol/vol); Gibco™), and heat-inactivated fetal bovine serum (10 % (vol/vol); Gibco™). The culture medium of B16-F10 cell line was further supplemented with MEM non-essential amino acid solution (1 % (vol/vol); Gibco™) and MEM vitamin solution (1 % (vol/vol); Gibco™). Cancer cells were cultured in a cell culture incubator (37 °C, 5 % CO_2, 95 % humidity; ESCO CCL-170B-8) using T75 cell culture flasks (Sarstedt ltd., Hungary). Tumor cell transplantation was obtained after five passages and the cell viability was verified with trypan blue exclusion test.

2.5. Experimental animals

CB17 SCID immunodeficient mice (12-week-old male mice were purchased from Innovo ltd., Hungary; n = 35) and Fischer-344 rats (16-week-old female rats were purchased from Innovo ltd., Hungary; n = 18) were used for the *in vivo* and *ex vivo* experiments. Animals were housed under sterile conditions in IVC cage system (Techniplast, Italy) at a temperature of 26 ± 3 °C, with 52 ± 10 % humidity and artificial lighting with a circadian cycle of 12 h. Sterile drinking water and semi-synthetic diet (Akronom ltd., Budapest, Hungary) were available *ad libitum* to all the animals. Laboratory animals were kept and treated in compliance with all applicable sections of the Hungarian Laws and regulations of the European Union (ethical permission numbers: III/6-KÁT/2015; 16/2020/DEMÁB).

2.6. Tumor models

For the induction of subcutaneous tumor models, cancer cells ($5x10^6$ cells) in 100 μL 0.9 % NaCl solution were injected subcutaneously into the left shoulder area of the experimental animals. *Ex vivo* and *in vivo* biodistribution studies were carried out 10 ± 2 days after subcutaneous injection of tumor cells at the tumor volume of 95 ± 8 mm^3.

To establish the Ne/De tumor-bearing metastasis model the subrenal capsule assay (SRCA) surgery was used (Trencsenyi et al., 2009). Rats were anaesthetized before the surgery by 1.5 % Forane, (AbbVie, Budapest, Hungary), 0.4 L/min O_2 and 1.2 L/min N_2O (Linde Healthcare, Budapest, Hungary) using an isoflurane anesthesia chamber (Eickemeyer Research, Tec3, Ghislandi ltd., Hungary). The left lumbar region was shaved and disinfected. The skin and the muscle layer were intersected to reach the left kidney. A small incision was made on the capsule renalis using Iris scissors, through which 1×10^6 Ne/De cells on Gelapson disk (Bausch & Lomb, Vaughan, Canada) in 10 μL 0.9 % NaCl saline solution were implanted under the left renal capsule of the rats.

2.7. Small animal PET imaging

Tumor-bearing animals were anaesthetized by 1.5 % isoflurane (Forane) with a dedicated small animal anesthesia device (Eickemeyer Research, Tec3, Ghislandi ltd., Hungary) and were injected with approximately 10 MBq of ^{18}FDG, ^{68}Ga-NODAGA-RAMEB or ^{68}Ga-NODAGA-HPβCD *via* the lateral tail vein. 50 (^{18}FDG) and 90 min (^{68}Ga-labelled RAMEB and HPβCD) after radiotracer injection, static PET images (20 min acquisition time/bed position) were acquired using the preclinical MiniPET-II scanner (University of Debrecen, Debrecen, Hungary).

2.8. PET data analysis

Ellipsoidal 3-dimensional volumes of interest (VOI) were manually drawn around the edge of the organ activity by visual inspection using BrainCad image analysis software (University of Debrecen, Debrecen, Hungary). For the quantitation of the radiotracer uptake in the experimental tumors and tissues, standardized uptake value (SUV) was calculated as follows: SUV = [VOI activity (Bq/mL)]/[injected activity (Bq)/animal weight (g)], assuming a density of 1 g/mL. Tumor-to-muscle (T/M) ratios were calculated from the SUVmean and SUVmax data of the tumors and the background (muscle).

2.9. Ex vivo studies

Tumor-bearing animals were injected with approximately 10 MBq of ^{68}Ga-NODAGA-RAMEB or ^{68}Ga-NODAGA-HPβCD. Ninety minutes after the intravenous injection of the radiopharmaceuticals animals were euthanized with 5 % isoflurane. Tumors were removed, and their weight and radioactivity were measured with a calibrated gamma counter (Perkin-Elmer Packard Cobra, Waltham, MA, USA). The radiotracer uptake was expressed as %ID/g tissue.

2.10. Immunohistochemistry

Four μm thick sections of the formaldehyde fixed and paraffin embedded experimental tumors were exposed to the rabbit monoclonal anti-Prostaglandin E Receptor EP2/PTGER2 antibody (Abcam, USA; cat. no.: ab167171) at a dilution of 1:1000 following deparaffination, rehydration and antigen retrieval (pH 6.0) as usual. An HRP-labelled anti-rabbit polymer antibody (Mach2, BioCare Medical, USA) and the Envision DAB detection kit (DAKO-Agilent Technologies, USA) were used for the visualization of the specific antibody binding, followed by hematoxylin counterstaining. In case of B16-F10 melanoma, VIP-Peroxidase (HRP) (ImmPACT® VIP Substrate, Peroxidase (HRP); Vector Laboratories, Newark, USA) was used for the visualization of the primary antibody. For microscopic imaging the Leica DM2500 research microscope equipped with DFC495 digital camera, and the LAS imaging software (Leica Microsystems, BioMarker ltd., Gödöllő, Hungary) were used.

2.11. Statistical analysis

Significance was calculated by two-way ANOVA, Student's *t*-test (two-tailed) and Mann-Whitney *U* test using the MedCalc 18.5 software package (MedCalc Software, Mariakerke, Belgium). The significance level was set at $p < 0.05$ unless otherwise indicated. Data are presented as mean ± SD of at least three independent experiments.

3. Results

3.1. Radiochemistry and determination of in vitro, in vivo metabolic stability

Radiolabelling of NODAGA-RAMEB and NODAGA-HPβCD CyDs was performed successfully by manual methodology. The average reaction time was approximately 20–25 min in both cases and the radiochemical purity (RCP) of products was over 98.0 %. The *in vitro* stability of ^{68}Ga-NODAGA-HPβCD and ^{68}Ga-NODAGA-RAMEB was analyzed in mouse serum using analytical radio-HPLC. Samples were taken at 30, 60, and 90 min and the HPLC results showed that both compounds remained stable over the measured time interval, with radiochemical purity exceeding 98 %. *In vivo* stability was tested in urine 60 min after radiotracer injection. Results indicated excellent *in vivo* metabolic stability, because none of the samples showed measurable amounts of radioactive metabolite. Radiochemical purity of the measured samples remained over 98 %.

3.2. In vivo PET imaging of subcutaneous tumor models

The tumor targeting properties and the PGE2 selectivity of ^{68}Ga-NODAGA-HPβCD and ^{68}Ga-NODAGA-RAMEB were investigated by *in vivo* PET imaging using subcutaneously growing experimental tumors 10 ± 2 days after tumor cell inoculation. Representative decay-corrected small animal PET images are shown in Fig. 1**A**. The qualitative analysis of PET images revealed that all the investigated subcutaneously transplanted tumors could be identified with ^{68}Ga-NODAGA-HPβCD and ^{68}Ga-NODAGA-RAMEB; however, there were significant differences in the extent of the accumulation. It was also observed that in some cases notable differences were found between the accumulation of the two ^{68}Ga-labelled radiopharmaceuticals in the same tumor (HT1080, A20, B16-F10). By analyzing the ^{18}FDG images, we found that HT1080, PancTu-1, and BxPC3 tumors showed markedly low radiopharmaceutical accumulation without any FDG avid regions. These visual observations were also confirmed by the quantitative SUV data analysis of the decay-corrected PET images (Fig. 1**B** and supplementary material **Table S1 and S2**).

3.3. In vivo PET imaging of SRCA-metastatic Ne/De tumor model

For the assessment of primary tumor and metastasis targeting properties of the ^{68}Ga-labelled CyDs, Ne/De tumor-bearing rats were used 8 days after Ne/De tumor cell implantation by subrenal capsule assay surgery. The presence of primary Ne/De tumor growing under the left kidney capsule and the thoracic parathymic lymph node (PTLN) metastases was confirmed by ^{18}FDG-PET imaging (Fig. 2). After the qualitative image analysis, we found that the primary tumors growing under the renal capsule could be well identified applying both ^{68}Ga-NODAGA-HPβCD and ^{68}Ga-NODAGA-RAMEB, however, the metastatic parathymic lymph node metastases were detectable only with the ^{68}Ga-NODAGA-conjugated HPβCD CyD (Fig. 2**A**). These visual observations were confirmed by the assessment of the quantitative SUV data. Approximately twofold higher ^{18}FDG uptake was observed than that of the ^{68}Ga-labelled probes, and this difference was significant at $p \leq 0.01$ (Fig. 2**B** and supplementary material **Table S3**). Nevertheless, regarding tumor-to-background ratio - that influences the evaluability of the PET images - we found no significant differences (at $p \leq 0.05$) between the ^{18}FDG and ^{68}Ga-labelled CyDs. Comparing the accumulation of the two radiolabelled CyDs in the primary Ne/De tumors, we found higher SUV values in case of ^{68}Ga-NODAGA-HPβCD (SUVmean: 3.52 ± 0.23; SUVmax: 4.80 ± 0.21), than ^{68}Ga-NODAGA-RAMEB, where the SUVmean and the SUVmax were 2.51 ± 0.19 and 3.21 ± 0.35, respectively. This lower ^{68}Ga-NODAGA-RAMEB accumulation was also observed in the metastatic parathymic lymph nodes, where approximately 2-fold higher SUV values were found with ^{68}Ga-NODAGA-HPβCD. In contrast to the primary tumor, in case of the parathymic lymph nodes the ^{18}FDG-T/M ratios were significantly ($p \leq 0.01$) higher compared to the ^{68}Ga-labelled radiopharmaceuticals. As for the radiolabelled CyD uptake in the primary and secondary tumors, significantly ($p \leq 0.01$) lower (approx. 3–5-fold) accumulation was observed in the metastases. Accordingly, immunohistochemical staining also showed lower PGE2 receptor expression in the parathymic lymph node (Fig. 2**C**).

3.4. Ex vivo radiotracer uptake of experimental tumors

For the assessment of tumor targeting potential of ^{68}Ga-NODAGA-HPβCD and ^{68}Ga-NODAGA-RAMEB *ex vivo* biodistribution studies were performed 90 min postinjection. Table 1 demonstrates that the *ex vivo* %ID/g data of the ^{68}Ga-NODAGA-conjugated CyDs correlate well with the *in vivo* SUV values. Similarly to the *in vivo* results, the PGE2 positive BxPC3, A20, Ne/De and He/De tumors showed the highest accumulation using both ^{68}Ga-labelled CyDs. In case of Ne/De tumors, significant difference ($p \leq 0.01$) was observed between the radiopharmaceutical uptake of the subcutaneously and the SRCA transplanted tumors.

3.5. Immunohistochemistry studies

The prostaglandin E receptor (EP2) expression of the subcutaneously growing experimental tumors was investigated by immunohistochemistry. In line with the *in vivo* and *ex vivo* radiotracer uptake results, strong EP2 receptor positivity was observed in the membrane of A20, BxPC3, B16-F10, Ne/De and He/De tumor cells, and lower signal intensity was observed in the HT1080 and PancTu-1 tumors with low prostaglandin E2 receptor expression (Fig. 3).

4. Discussion

The aim of this present study was to evaluate the tumor-targeting ability of ^{68}Ga-labelled HPβCD and RAMEB CyDs and find an association between PGE2 production and radiopharmaceutical uptake in the investigated experimental tumors using preclinical PET. *In vivo* PET imaging revealed that all investigated subcutaneously transplanted tumors could be identified with ^{68}Ga-NODAGA-HPβCD and ^{68}Ga-NODAGA-RAMEB; however, significant differences were encountered between the extents of the tracer accumulation (Fig. 1). This observation might be explained by either the different EP receptor profile of the examined tumors and the different PGE2 concentrations in the given tumor niche. However, to our best knowledge, no exact data are available in the current literature regarding the PGE2 receptor expression of the investigated tumors; previous research has already strengthened the presence of EP receptors and PGE2 in some cell lines. Yip-Schneider (2000) reported about the elevated levels of PGE2 production in BxPC3 human pancreatic adenocarcinoma cell line (Yip-Schneider, 2000). Furthermore, other workgroups pinpointed that the activation of EP1 and EP2 receptors requires significantly higher levels of PGE2 (O'Callaghan and Houston, 2015). In another study, conducted by Takahashi and colleagues (2015), enhanced PGE2 secretion and high EP2 receptor expression were experienced in BxPC3 cell line during characterization of different human pancreatic cancer cells utilizing *in vitro* assays (Takahashi et al., 2015). As for PancTu-1 cell lines, very low COX2 expression and PGE2 production were observed in a research evaluating different pancreatic ductal adenocarcinoma cells by flow cytometry and western blot analysis (Gonnermann et al., 2015). Our previous results are in line with the previously mentioned ones, since verified by immunohistochemistry we observed remarkable presence of EP2 receptors in BxPC3 tumors, and lower receptor expression in PancTu-1 tumors, confirming that subcutaneously growing BxPC3 tumors retained this property *in vivo* (Trencsényi et al., 2020). Although the EP receptor profile of the HT1080 fibrosarcoma cells is not yet fully elucidated, according to the results of a study in which the effect of 5-azacytidine on COX2 expression and PGE production was assessed, we suggest the presence of EP receptors on HT1080 cells (Yu and Kim, 2015). In addition, with the application of B16-F10 melanoma cell lines, Kim and co-workers (2016) investigated the influence of timosaponin AIII - a compound derived from Anemarrhena asphodeloides Bunge - on cancer cell migration. While the upregulation of COX2 and related PGE2 and EP receptors promote melanoma cell migration *in vitro*, administration of timosaponin AIII led to the inhibition of cell migration in association with a decrease in COX2, PGE2 and EP receptor expression (Kim et al., 2016). Even though no existing research ensure quantitative data on the receptor expression profile of B16-F10 cell lines, based on the results of the above detailed study we may hypothesize considerable EP receptor and PGE2 expression of B16-F10 melanoma cells. Regarding A20 cell lines no study dealing with their EP receptor status is available so far, however, Fedyk and colleagues (1996) investigated the expression of different subtypes of EP receptors of B-lymphocytes in the following cell lines: 702/3, CH3 1, CH33, ECH408.1, WEHI-231, CH 12 and CH27. Applying real-time polymerase chain reaction (RT-PCR), northern blot and DNA sequencing analysis, mRNA encoding EP1, EP3beta and EP4 subtypes of PGE receptors were identified on transformed B lymphocytes (Fedyk et al., 1996). Since former literature data revealed the

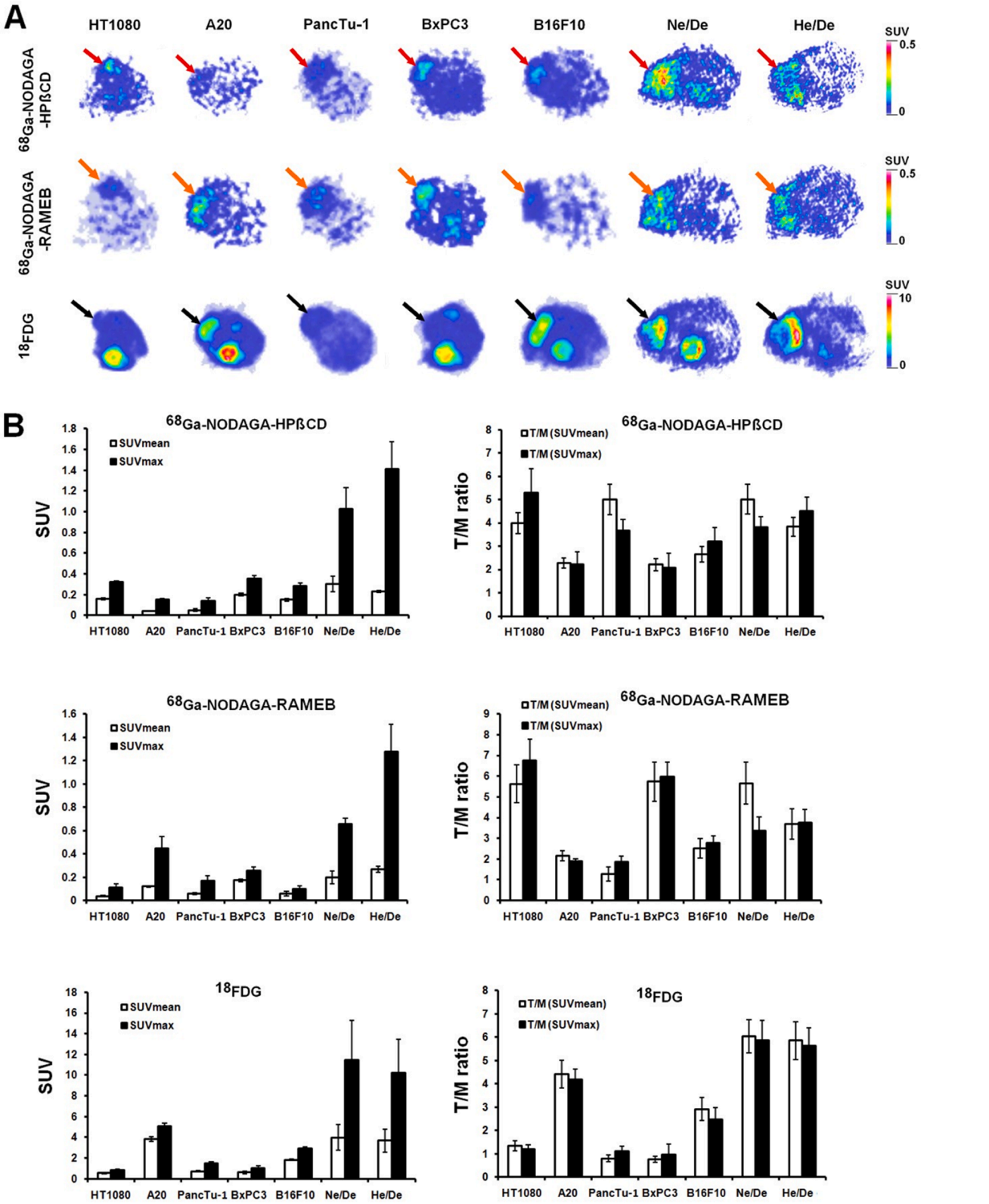

Fig. 1. Representative decay-corrected transaxial PET images of experimental tumors after the intravenous injection of ^{68}Ga-NODAGA-HPβCD (red arrows), ^{68}Ga-NODAGA-RAMEB (orange arrows), and ^{18}FDG (black arrows) (A). Quantitative SUV data analysis of the PET images (B). PET images and SUV data were obtained 10 ± 2 days after subcutaneous tumor cell inoculation, and 50 and 90 min after the intravenous injection of ^{18}FDG and ^{68}Ga-labelled probes, respectively. SUV: standardized uptake value; T/M: tumor-to-muscle ratio. SUV values are presented as mean ± SD. (For interpretation of the references to colour in this figure legend, the reader is referred to the web version of this article.)

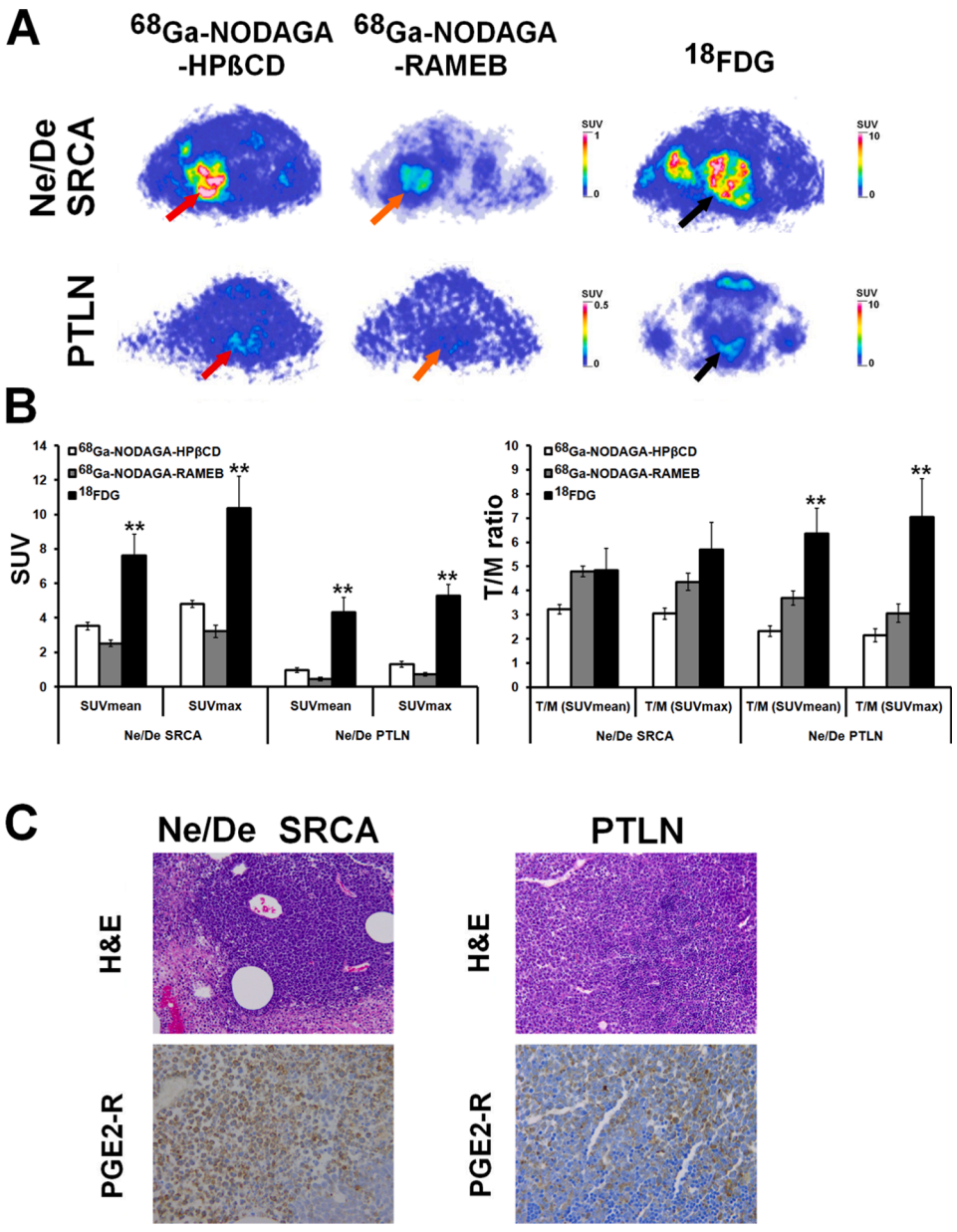

Fig. 2. *In vivo* assessment of ^{68}Ga-NODAGA-HPβCD (red arrows), ^{68}Ga-NODAGA-RAMEB (orange arrows), and ^{18}FDG (black arrows) accumulation of Ne/De primary tumors (SRCA) and parathymic lymph node (PTLN) etastases using miniPET imaging (A). Quantitative SUV data analysis of the PET images (B). PET images and SUV data were obtained 8 days after the subrenal capsule assay surgery (SRCA), and 50 and 90 min after the intravenous injection of ^{18}FDG and ^{68}Ga-labelled probes, respectively. SUV: standardized uptake value; T/M: tumor-to-muscle ratio. SUV values are presented as mean ± SD. Significance level between ^{18}FDG and the ^{68}Ga-labelled probes: $p \leq 0.01$ (*). Histological analysis of Ne/De primary tumors (SRCA) and parathymic lymph node (PTLN) metastasis. Upper row: Representative hematoxylin-eosin (H&E) stained tumor tissue. Magnification: 20X. Lower row: anti-Prostaglandin E Receptor EP2/PTGER2 antibody immunohistochemistry (PGE2-R), visualized with 3,3-diaminobenzidine (DAB) (brown staining). Magnification: 40X. (For interpretation of the references to colour in this figure legend, the reader is referred to the web version of this article.)

presence of PGE2 receptors on several B-cell lines, we suppose that A20 cell lines probably also show some expression. Despite the fact that receptor expression of the tumor cell lines may suggest some associations with ^{68}Ga-labelled RAMEB and HPβCD accumulation, large scale future studies are warranted to fully strengthen the connection between the receptor profile of the tumors and the radiopharmaceutical uptake.

In studies with ^{18}FDG, it was observed that HT1080, PancTu-1, and BxPC3 tumors showed low radiopharmaceutical accumulation with ^{18}FDG, which is widely used for tumor imaging and staging. Earlier clinical and preclinical studies have also reported that - due to the low cellularity, low glucose metabolism and glucose transporter expression or small tumor size - certain tumor types (e.g.: well-differentiated thyroid and neuroendocrine tumors, low-grade lung adenocarcinoma, renal cell cancers) are not ^{18}FDG avid or very low uptake was found. In these cases, it may be particularly appropriate to use a more specific radiopharmaceutical that targets another property of the cancer (Flavell et al., 2016; Hofman and Hicks, 2016).

In this present work, the tumor targeting potential of ^{68}Ga-labelled CyDs was also investigated using Ne/De tumor-bearing rats 8 days after tumor cell implantation by subrenal capsule assay (SRCA) surgery. The peculiarity of this metastasis animal model is that cells transplanted under the renal capsule metastasize to the parathymic lymph node in the thorax within a week. In our study, we performed syngenic-orthotopic transplantation, according to which mesoblastic nephroma (Ne/De) tumor cells derived from F-344 rats were implanted under the renal capsule of rats from the same strain (Máté et al., 2015; Trencsenyi et al., 2009). After confirming the presence of primary Ne/De tumors growing under the left kidney capsule and the parathymic lymph node (PTLN) metastases by ^{18}FDG-PET imaging, we found approximately 5–10-fold higher ^{68}Ga-labelled radiotracer uptake (Fig. 2 and Supplementary material **Table S3**), than that of the subcutaneous Ne/De tumor model (Fig. 1 and Supplementary material **Table S1**). The explanation for this phenomenon is that the subcutaneous transplantation is lacking in orthotopic tissue microenvironment. In contrast, in the SRCA model, tumor cells were implanted at orthotopic site with favorable microenvironment, which promotes tumor cell proliferation and the development of distant metastases (Borgstrom et al., 2013). Similar results were found by our research group, when the expression of neoangiogenic

Table 1
Ex vivo assessment of ^{68}Ga-NODAGA-HPβCD and ^{68}Ga-NODAGA-RAMEB accumulation (%ID/g) in experimental tumors 10 ± 2 days after tumor induction and 90 min after intravenous radiotracer injection. Significance level between subcutaneously (sc.) and SRCA induced primary and metastatic Ne/De tumors at 90 min: $p \leq 0.01$ (*). SRCA: subrenal capsule assay surgery induced tumor. PTLN: parathymic lymph node metastasis. %ID/g values are presented as mean ± SD.

	^{68}Ga-NODAGA-HPβCD (90 min)	^{68}Ga-NODAGA-RAMEB (90 min)
HT1080	0.20 ± 0.05	0.09 ± 0.02
A20	0.06 ± 0.03	0.15 ± 0.07
PancTu	0.08 ± 0.03	0.10 ± 0.02
BxPC3	0.30 ± 0.06	0.36 ± 0.07
B16F10	0.21 ± 0.09	0.32 ± 0.10
Ne/De sc.	0.41 ± 0.09	0.36 ± 0.08
He/De sc.	0.35 ± 0.08	0.43 ± 0.11
Ne/De SRCA	2.45 ± 0.41*	2.13 ± 0.37*
Ne/De PTLN	1.75 ± 0.27*	1.52 ± 0.19*

molecules was compared in subcutaneously and SRCA surgery induced Ne/De tumors (Máté et al., 2015).

Regarding the results of immunohistochemistry, strong EP2 receptor positivity was observed in the membrane of A20, BxPC3, B16-F10, Ne/De and He/De tumor cells while in case of HT1080, and PancTu-1 tumors characterized by lower receptor expression lower signal intensity was detected. Upon visual assessment, we experienced that PGE2 positivity was more prominent compared to the receptor positivity identified on the immunohistochemical slices. Change in the receptor expression of the tumor cells during tumor progression may explain this phenomenon. Tumor growth is featured with the appearance of necrosis, chronic inflammation and chronic as well as cyclic hypoxia that show positive correlation with both PGE2 production and PGE2 receptor expression (Nasry and Martin, 2021). In our study, PET acquisition of the experimental animals occurred 10–12 days postinjection. Therefore, we hypothesize that there has not yet been such a great extent of tumor dedifferentiation and related PGE2 receptor upregulation that would have been so noticeable with staining. Another thing to consider is that staining is specific to the receptor, while ^{68}Ga-labelled CyDs indicate both PGE2 alone and PGE2 attached to its receptor. Thus, with PET imaging we could visually register stronger positivity since it detects PGE2 (alone or with receptor), while staining only shows the receptor, the amount of which – based on the previous literature data – was probably not so explicit in our tumors.

5. Conclusion

^{68}Ga-labelled CyDs may open a novel field in the PET diagnostics of PGE2 positive primary tumors and metastases. Although the PGE2 receptor expression of the investigated tumors is associated with the ^{68}Ga-labelled RAMEB and HPβCD accumulation, large scale future studies are warranted to fully strengthen the connection between the receptor profile of the tumors and the radiopharmaceutical uptake.

CRediT authorship contribution statement

Judit P. Szabó: Visualization, Investigation, Conceptualization, Writing – original draft. **Katalin Csige:** Methodology, Visualization, Investigation. **Ibolya Kálmán-Szabó:** Methodology. **Viktória Arató:** Methodology. **Gábor Opposits:** Methodology, Visualization, Investigation. **István Jószai:** Methodology, Visualization, Investigation. **István Kertész:** Writing – review & editing. **Zita Képes:** Methodology, Writing – review & editing. **Gábor Méhes:** Methodology. **Ferenc Fenyvesi:** Validation. **István Hajdu:** Conceptualization, Writing – review & editing. **György Trencsényi:** Writing – review & editing, Supervision.

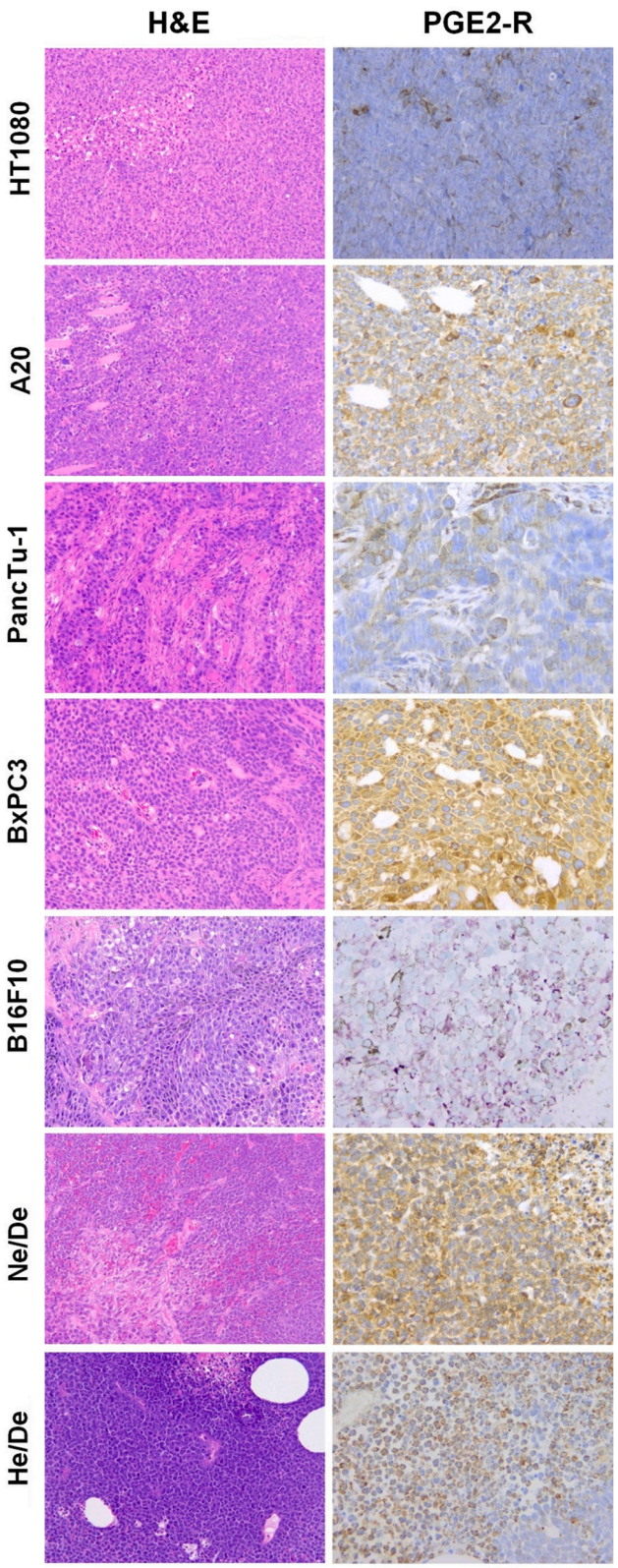

Fig. 3. Histological analysis of subcutaneously growing experimental tumors 10 ± 2 days after tumor cell inoculation. Upper row: Representative hematoxylin-eosin (H&E) stained tumor tissue. Magnification: 20X. Lower row: anti-Prostaglandin E Receptor EP2/PTGER2 antibody immunohistochemistry (PGE2-R), visualized with 3,3-diaminobenzidine (DAB) (brown staining) and VIP peroxidase (purple staining; B16-F10 melanoma). Magnification: 40X. (For interpretation of the references to colour in this figure legend, the reader is referred to the web version of this article.)

Declaration of Competing Interest

The authors declare that they have no known competing financial interests or personal relationships that could have appeared to influence the work reported in this paper.

Data availability

Data will be made available on request.

Acknowledgements

This study was supported by FK_17 (FK124634) research grant of the National Research Development and Innovation Office, Budapest, Hungary, by the János Bolyai Research Scholarship of the Hungarian Academy of Sciences (BO/328/21, BO/00365/15 and BO/00290/16), and by the Thematic Excellence Programme (TKP2020-NKA-04) of the Ministry for Innovation and Technology in Hungary. PhD students were supported by the University of Debrecen, Doctoral School of Pharmaceutical Sciences (EFOP-3.6.3-VEKOP-16-2017-00009 grant) and Doctoral School of Clinical Medicine.

Appendix A. Supplementary material

Supplementary data to this article can be found online at https://doi.org/10.1016/j.ijpharm.2022.122462.

References

Borgstrom, P., Oh, P., Czarny, M., Racine, B., Schnitzer, J.E., 2013. Co-implanting orthotopic tissue creates stroma microenvironment enhancing growth and angiogenesis of multiple tumors. F1000Research 2, 129. https://doi.org/10.12688/f1000research.2-129.v2.

Chelly, J.E., Singla, S.K., Melson, T.I., Lacouture, P.G., Paadre, S., Carr, D.B., 2013. Safety of a novel parenteral formulation of diclofenac after major orthopedic or abdominal/pelvic surgery in a population including anticoagulated, elderly or renally insufficient patients: an open-label, multiday, repeated dose clinical trial. Pain Med. 14, 749–761. https://doi.org/10.1111/pme.12076.

C.D, Davidson, N.F, Ali, M.C, Micsenyi, G, Stephney, S, Renault, K, Dobrenis, D.S, Ory, M. T, Vanier, S.U, Walkley, Chronic cyclodextrin treatment of murine Niemann-Pick C disease ameliorates neuronal cholesterol and glycosphingolipid storage and disease progression. PLoS One. 4.2009 https://doi.org/10.1371/journal.pone.0006951.

Duchene, D., Cavalli, R., Gref, R., 2016. Cyclodextrin-based polymeric nanoparticles as efficient carriers for anticancer drugs. Curr. Pharm. Biotechnol. 17, 248–255. https://doi.org/10.2174/1389201017666151030104944.

Fedyk, E.R., Ripper, J.M., Brown, D.M., Phipps, R.P., 1996. A molecular analysis of PGE receptor (EP) expression on normal and transformed B lymphocytes: Coexpression of EP1, EP2, EP3β and EP4. Mol. Immunol. 1, 33–45. https://doi.org/10.1016/0161-5890(95)00130-1.

Flavell, R.R., Naeger, D.M., Mari, A.C., Hawkins, R.A., Pampaloni, M.H., Behr, S.C., 2016. Malignancies with low fluorodeoxyglucose uptake at PET/CT: Pitfalls and prognostic importance: resident and fellow education feature. Radiographics. 1, 293–294. https://doi.org/10.1148/rg.2016150073.

D, Gonnermann, H.H, Oberg, C, Kellner, M, Peipp, S, Sebens, D, Kabelitz, D, Wesch, Resistance of cyclooxygenase-2 expressing pancreatic ductal adenocarcinoma cells against γδ T cell cytotoxicity. Oncoimmunology. 4 2015, e988460. https://doi.org/10.4161/2162402X.2014.988460.

Gould, S., Scott, R.C., 2005. 2-Hydroxypropyl-β-cyclodextrin (HP-β-CD): a toxicology review. Food Chem. Toxicol. 43, 1451–1459. https://doi.org/10.1016/j.fct.2005.03.007.

Hajdu, I., Angyal, J., Szikra, D., Kertész, I., Malanga, M., Fenyvesi, É., Szente, L., Vecsernyés, M., Bácskay, I., Váradi, J., Fehér, P., Ujhelyi, Z., Vasvári, G., Rusznyák, Á., Trencsényi, G., Fenyvesi, F., 2019. Radiochemical synthesis and preclinical evaluation of 68Ga-labeled NODAGA-hydroxypropyl-beta-cyclodextrin (68Ga-NODAGA-HPBCD). Eur. J. Pharm. Sci. 128, 202–208.

Hastings, C., Vieira, C., Liu, B., Bascon, C., Gao, C., Wang, R.Y., Casey, A., Hrynkow, S., 2019. Expanded access with intravenous hydroxypropyl-β-cyclodextrin to treat children and young adults with Niemann-Pick disease type C1: a case report analysis. Orphanet J. Rare Dis. 14, 228. https://doi.org/10.1186/s13023-019-1207-1.

Hofman, M.S., Hicks, R.J., 2016. How we read oncologic FDG PET/CT. Cancer Imaging. 16, 35. https://doi.org/10.1186/s40644-016-0091-3.

Karpisheh, V., Nikkhoo, A., Hojjat-Farsangi, M., Namdar, A., Azizi, G., Ghalamfarsa, G., Sabz, G., Yousefi, M., Yousefi, B., Jadidi-Niaragh, F., 2019. Prostaglandin E2 as a potent therapeutic target for treatment of colon cancer. Prostaglandins Other Lipid Mediat. 144, 106338.

Kim, K.M., Im, A., Kim, S.H., Hyun, J.W., Chae, S., 2016. Timosaponin AIII inhibits melanoma cell migration by suppressing COX-2 and in vivo tumor metastasis. Cancer Sci. 107, 181–188. https://doi.org/10.1111/cas.12852.

Loftsson, T., Jarho, P., Másson, M., Järvinen, T., 2005. Cyclodextrins in drug delivery. Expert Opin. Drug. Deliv. 2, 335–351. https://doi.org/10.1517/17425247.2.1.335.

Máté, G., Kertész, I., Enyedi, K.N., Mező, G., Angyal, J., Vasas, N., Kis, A., Szabó, É., Emri, M., Bíró, T., Galuska, L., Trencsényi, G., 2015. In vivo imaging of Aminopeptidase N (CD13) receptors in experimental renal tumors using the novel radiotracer 68Ga-NOTA-c(NGR). Eur. J. Pharm. Sci. 69, 61–71.

Nasry, W.H.S., Martin, C.K., 2021. Intersecting mechanisms of hypoxia and prostaglandin E2-mediated inflammation in the comparative biology of oral squamous cell carcinoma. Front. Oncol. 11, 539361 https://doi.org/10.3389/fonc.2021.539361.

O'Callaghan, G., Houston, A., 2015. Prostaglandin E2 and the EP receptors in malignancy: possible therapeutic targets? Br. J. Pharmacol. 172, 5239–5250. https://doi.org/10.1111/bph.13331.

E., Ottinger, M, Kao, N, Carrillo-Carrasco, N, Yanjanin, R, Shankar, M, Janssen, M, Brewster, I, Scott, X, Xu, J, Cradock, P, Terse, S.J, Dehdashti, J, Marugan, W, Zheng, L, Portilla, A, Hubbs, WJ, Pavan, J, Heiss, C.H, Vite, S.T, Walkley, D.S, Ory, S.A, Silber, F.D, Porter, C.P, Austin, J.C, McKew, Collaborative ddevelopment of 2-Hydroxypropyl -β-Cyclodextrin for the treatment of Niemann-Pick type C1 disease. Curr. Top. Med. Chem. 14 2014, 330 339. https://doi.org/ 10.2174/1568026613666131127160118.

Sauer, R.S., Rittner, H.L., Roewer, N., Sohajda, T., Shityakov, S., Brack, A., Broscheit, J. A., 2017. A novel approach for the control of inflammatory pain: Prostaglandin E2 complexation by randomly methylated β-cyclodextrins. Anesth. Analg. 124, 675–685. https://doi.org/10.1213/ANE.0000000000001674.

Szejtli, J., 1998. Introduction and general overview of cyclodextrin chemistry. Chem. Rev. 98, 1743–1754. https://doi.org/10.1021/cr970022c.

Takahashi, T., Uehara, H., Ogawa, H., Umemoto, H., Bando, Y., Izumi, K., 2015. Inhibition of EP2/EP4 signaling abrogates IGF-1R-mediated cancer cell growth: Involvement of protein kinase C-θ activation. Oncotarget. 6, 4829–4844. https://doi.org/10.18632/oncotarget.3104.

Trencsényi, G., Kertai, P., Bako, F., Hunyadi, J., Marian, T., Hargitai, Z., Pocsi, I., Muranyi, E., Hornyak, L., Banfalvi, G., 2009. Renal capsule-parathymic lymph node complex: a new in vivo metastatic model in rats. Anticancer Res. 29, 2121–2126.

Trencsényi, G., Kis, A., Szabó, J.P., Ráti, Á., Csige, K., Fenyvesi, É., Szente, L., Malanga, M., Méhes, G., Emri, M., Kertész, I., Vecsernyés, M., Fenyvesi, F., Hajdu, I., 2020. In vivo preclinical evaluation of the new 68Ga-labeled beta-cyclodextrin in prostaglandin E2 (PGE2) positive tumor model using positron emission tomography. Int. J. Pharm. 576, 118954 https://doi.org/10.1016/j.ijpharm.2019.118954.

Vite, C.H., Bagel, J.H., Swain, G.P., Prociuk, M., Sikora, T.U., Stein, V.M., O'Donnell, P., Ruane, T., Ward, S., Crooks, A., Li, S., Mauldin, E., Stellar, S., De Meulder, M., Kao, M.L., Ory, D.S., Davidson, C., Vanier, M.T., Walkley, S.U., 2015. Intracisternal cyclodextrin prevents cerebellar dysfunction and Purkinje cell death in feline Niemann-Pick type C1 disease. Sci. Transl. Med. 7 https://doi.org/10.1126/scitranslmed.3010101.

Yip-Schneider, M.T., 2000. Cyclooxygenase-2 expression in human pancreatic adenocarcinomas. Carcinogenesis. 1, 139–146. https://doi.org/10.1093/carcin/21.2.139.

S.M, Yu, S.J, Kim, DNA-hypomethylating agent, 5′-azacytidine, induces cyclooxygenase-2 expression via the PI3-kinase/Akt and extracellular signal-regulated kinase-1/2 pathways in human HT1080 fibrosarcoma cells. Int. J. Oncol. 47 2015, 1469 1475 10.3892/ijo.2015.3110.